Structure, Properties, and Bonding of ZrTe (MnP Type), a Low-Symmetry, High-Temperature Modification of ZrTe (WC Type)

Gissur Örlygsson and Bernd Harbrecht*

Contribution from the Department of Chemistry and Materials Science Centre, Philipps University, Hans-Meerwein-Strasse, D-35032 Marburg, Germany

Received December 4, 2000

Abstract: ZrTe (*MnP*) was synthesized by high-temperature methods at 1570 K in Ta ampules. The structure of the telluride was determined by means of single-crystal X-ray diffraction to be orthorhombic, *Pnma* (No. 62), $Z = 4$, Pearson Symbol *oP*8, $a = 739.15(15)$ pm, $b = 377.23(8)$ pm, $c = 694.34(14)$ pm. The orthorhombic MnP type structure is a distorted variant of the NiAs type structure with pronounced metal−metal zigzag chains. Zigzag chains are typical for phases with a d^2 metal atom electron configuration. According to extended Hückel calculations, the homonuclear interactions in the zigzag chains make up for $^2/_3$ of the Zr−Zr interactions in ZrTe (*MnP*) and contribute decisively to the stability of the structure. The emergence of the distorted MnP type structure instead of the high-symmetry NiAs type ZrTe at high temperatures can be understood as the result of an optimization of homonuclear Zr−Zr interactions arising from states close to the Fermi level. The hexagonal WC type ZrTe transforms above 1438 ± 5 K into ZrTe (*MnP*) ($\Delta H = 8.3 \pm 1.0$ kJ mol^{-1}). The phase transition is reversible, although at room-temperature the reverse reaction is kinetically inhibited. Zr_5Te_4 and Zr_5Te_6 are the phases next to ZrTe. ZrTe (*MnP*) exhibits temperature-independent paramagnetic properties ($\chi_{mol} = 0.14 \times 10^{-3}$ cm^3 mol^{-1}), as typical for a metallic conductor. Resistivity measurements on ZrTe (*MnP*) imply metallic behavior.

Introduction

The study of phase transitions between structurally simple solid-state compounds offers interesting opportunities to gain insight into the factors stabilizing each phase and thereby into the driving forces underlying the structural changes. Binary, equiatomic phases are in this regard the ideal candidates, second only to the elements themselves.

The structure type pairs NaCl−WC, MnP−NiAs, and NiAs−WC, for example, belong to this category. Transition-metal carbides and nitrides often crystallize in the NaCl or the WC type structures. Theoretical calculations have shown that the valence-electron count per unit cell has a significant impact on the preference for one or the other of the two structure types.[1] A close relationship between structure and valence-electron count is also observed in transition-metal phosphides. In those compounds the driving force for transitions between NiAs and MnP type phases was found to be a second-order Jahn−Teller-like distortion.[2] The role of the valence-electron concentration has been substantiated in experiments in the ternary chalcogenide system Ti−V−S. Thus, as a result of a reduction in valence-electron concentration from 11 to ca. 10.5, $Ti_xV_{1-x}S$ transforms from the MnP type to the NiAs type when x lies above ca. 0.5.[3,4]

The MnP type structure[5] can be seen as an orthorhombically distorted variant of the NiAs type structure with pronounced metal atom zigzag chains. The MnP type often represents a second modification of phases of the NiAs type, e.g., for VS,[6,7] TiSe,[3,8] and CrAs,[9] in which the NiAs type corresponds to the high-temperature form. On the opposite side, NbS stabilizes at high temperatures in the MnP type, whereas at lower temperatures a hexagonal NiAs type superstructure exists.[10] In FeS, the MnP type structure can be induced through the application of high pressure.[11] Variations in stoichiometry apparently play a certain role in at least some of those phase transitions, e.g., ref 7.

In recent years, a number of new phases have been discovered in the system Zr−Te. In the metal-rich part of the system, Zr_3Te[12] and Zr_2Te[13] were characterized, whereas on the tellurium-rich side, Zr_5Te_6[14] and $Zr_{1.3}Te_2$[15] were identified. Furthermore, a reinvestigation of the phase diagram was carried out lately.[16] We report here on a new, binary zirconium telluride crystallizing in the MnP type structure. It represents a high-temperature modification of ZrTe. The low-temperature form crystallizes in the well-known WC type structure.[17,18] To our knowledge, a WC−MnP type phase transition has not been reported before. On this ground, and due to the structural simplicity of both compounds, we also have embarked on a study of the phase

(1) Wijeyesekera, S. D.; Hoffmann, R. *Organometallics* **1984**, *3*, 949.
(2) Tremel, W.; Hoffmann, R.; Silvestre, J. *J. Am. Chem. Soc.* **1986**, *108*, 5174.
(3) Henderson Lewis, L.; Goodenough, J. B. *J. Solid State Chem.* **1995**, *114*, 346.
(4) Franzen, H. F.; Leebrick, D. H.; Laabs, F. *J. Solid State Chem.* **1975**, *13*, 307.
(5) Rundqvist, S. *Acta Chem. Scand.* **1962**, *16*, 287.
(6) Franzen, H. F.; Wiegers, G. A. *J. Solid State Chem.* **1975**, *13*, 114.
(7) Silvestre, J.; Tremel, W.; Hoffmann, R. *J. Less-Common Metals* **1986**, *116*, 113.
(8) Grønvold, F.; Langmyhr, F. J. *Acta Chem. Scand.* **1961**, *15*, 1949.
(9) Selte, K.; Kjekshus, A. *Acta Chem. Scand.* **1973**, *27*, 3195.
(10) Kadijk, F.; Jellinek, F. *J. Less-Common Metals* **1969**, *19*, 421.
(11) King, H. E., Jr.; Prewitt, C. T. *Acta Crystallogr.* **1982**, *B38*, 1877.
(12) Harbrecht, B.; Leersch, R. *J. Alloys Compd.* **1996**, *238*, 13.
(13) Örlygsson, G.; Harbrecht, B. *Inorg. Chem.* **1999**, *38*, 3377.
(14) Örlygsson, G.; Harbrecht, B. *Chem. Eur. J.* **2000**, *6*, 4170.
(15) Wang, C.; Eylem, C.; Hughbanks, T. *Inorg. Chem.* **1998**, *37*, 390.
(16) de Boer, R.; Cordfunke, E. H. P. *J. Alloys Compd.* **1997**, *259*, 115.
(17) Brattås, L.; Kjekshus, A. *Acta Chem. Scand.* **1971**, *25*, 2350.
(18) Örlygsson, G.; Harbrecht, B. *Z. Naturforsch.* **1999**, *54b*, 1125.

10.1021/ja004164r CCC: $20.00
Published on Web 04/13/2001

transition and the factors governing the relative stability of each phase, as well as on a study of the structure−property relations.

Experimental Section

Preparation. Due to the air-sensitivity of the tellurides, they were stored and handled under argon. The starting material $ZrTe_2$ was prepared from the elements (Te 99.999%, Fluka; Zr 99.8%, ChemPur, $n_{Zr}:n_{Te} = 1:2$) in previously outgassed, sealed quartz glass tubes (1150 K, 1 d). Single crystals of ZrTe (*MnP*) were obtained through the reduction of $ZrTe_2$ with Zr ($n_{Zr}:n_{Te} = 1:1$; 1570 K, 3 d, I_2) in a sealed, argon-filled tantalum tube, which in turn was contained in an evacuated corundum tube ($P < 10^{-3}$ Pa). The temperature of the reaction mixture was uniformly raised at 100 K h^{-1} to 1570 K, and lowered again at 150 K h^{-1} to room temperature. By means of energy dispersive analysis of emitted X-rays (CamScan CS 4DV, EDX system, Noran Instruments; 30 kV, Zr-L, Te-L; detection limit: Be) no other elements than Zr and Te were found.

DSC Investigations. Differential scanning calorimetry (DSC) investigations were performed with the help of a SETARAM Setsys 16/18 with PtRh 6%/PtRh 30% thermocouples. The samples, 20−80 mg, were pressed into pellets (∅ 3.5 mm, 6.5 kN), and put in a molybdenum crucible, which subsequently was sealed under an argon atmosphere. The sample crucible, together with an empty reference crucible, was placed on the DSC transducer. The furnace compartment was evacuated ($P < 1$ Pa) and flooded with purified argon. This procedure was repeated three times before a measurement was conducted under a stream of purified argon. The heating rate used was 10 K min^{-1}; cooling rates were 10−40 K min^{-1}. No significant weight changes of the molybdenum crucibles were detected. Reactions between molybdenum and the specimens were not observed.

The calibration of the DSC transducer was achieved with the measurement of the temperature and heat of fusion of Au (ca. 10 mg; 99.99%, SETARAM) in open Mo crucibles. Au melts at 1337 K, $\Delta_{fus}H^0_{1337} = 12.55$ kJ mol^{-1}.[19] Only the heating peaks of the DSC experiments were used for evaluation, both in calibration measurements and in sample measurements.

Powder X-ray Diffraction. Guinier X-ray powder diffraction was used as a characterization method for phase identification. Guinier photographs were obtained with a Huber Guinier System 600 employing Cu $K\alpha_1$ radiation. Silicon[20] was added to the samples as an internal standard. Lattice parameters were determined from Guinier diffraction data by least-squares refinement with use of the local program DIFFRAKT.[21] X-ray powder diffractograms were recorded in reflection at ambient temperature on a Philips X'Pert MPD diffractometer with Bragg−Brentano geometry, equipped with a diffracted-beam curved graphite monochromator, using Cu Kα radiation (40 kV, 40 mA). Intensities were detected by means of a scintillation counter. An X-ray powder diffraction pattern and a Rietveld profile fit for a ZrTe (*MnP*) sample are shown in Figure 1.

Single-Crystal X-ray Diffraction. The selected, rectangularly shaped crystals with a silver luster were mounted in argon-filled glass capillaries. A data set of a suitable crystal was collected on an IPDS diffractometer (Stoe) at room temperature. Data reduction was performed with the IPDS-software, X-RED and X-SHAPE.[22] The structure was refined by using the program SHELXL-97.[23] Selected data for the single-crystal X-ray structure investigation of ZrTe (*MnP*) are given in Table 1. Positional parameters and isotropic, equivalent temperature factors, as well as anisotropic temperature factors, are given in Table 2. Selected interatomic distances may be found in Table 3. A numerical absorption correction resulted in a significant improvement of the final residual factors (before correction: $R(F_o) = 0.0248$; $R_w(F_o^2) = 0.0629$).

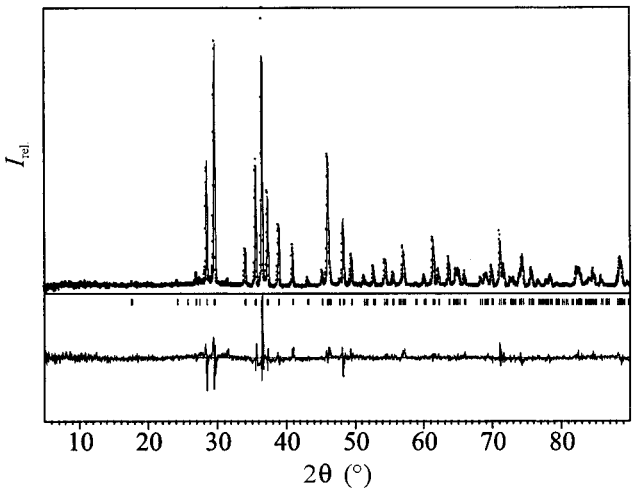

Figure 1. X-ray powder diffractogram (Cu Kα, relative intensities vs 2θ) and a Rietveld profile fit for ZrTe (*MnP*). Measured (dots) and calculated (line) intensities with a difference plot (bottom, 50% expanded). In the middle are shown the positions of the Bragg angles of ZrTe (*MnP*).

Table 1. Selected Crystallographic Data for ZrTe (*MnP*)

chemical formula	ZrTe
fw (g mol^{-1})	218.824
space group	orthorhombic, *Pnma* (No. 62)
Z	4
a (pm)	739.15(15)
b (pm)	377.23(8)
c (pm)	694.34(14)
V (10^6 pm^3)	193.60(7)
ρ_{calcd} (g cm^{-3})	7.507
μ (mm^{-1})	19.90
$R(F_o)^a$ ($I_o > 2\sigma(I_o)$); $R(F_o)$	0.0212; 0.0215
$R_w(F_o^2)^b$	0.0519
goodness of fit	1.208

[a] $R(F_o) = \sum||F_o| - |F_c||/\sum|F_o|$. [b] $w = 1/[\sigma^2(F_o^2) + (0.0294P)^2 + 0.5079P]$; $P = (F_o^2 + 2F_c^2)/3$.

The lattice parameters determined for the single crystal on the basis of the positions of 3024 reflections and those from Guinier powder diffraction data (38 reflections, $a = 738.09(8)$ pm, $b = 376.92(3)$ pm, $c = 694.09(8)$ pm) are in fair agreement. No signs of a partial occupation of the atomic sites were found.

Electrical Resistivity Measurements. The temperature dependence of the electrical resistivity of ZrTe (*MnP*) was determined between 10 and 300 K on a cold-pressed powder sample (13.0 × 2.0 × 1.25; length × width × thickness, mm) applying a four-probe dc method.[24] The sample was fixed on a mica plate which in turn was brought onto a copper plate to ensure good thermal contact with the coldfinger of the apparature. Contact wires of gold were attached to the sample with a silver paste. To compensate for errors due to thermal stress, the resistivity was measured by using both current directions ($I = 8$ mA). To check for hysteresis effects, the resistivity was measured upon cooling as well as upon heating.

Magnetic Susceptibility Measurements. Magnetic susceptibility measurements were carried out with the aid of a Quantum Design MPMS SQUID magnetometer with a He cryostat. The data were corrected for diamagnetism of sample holders and atom cores.[25] Powdered samples of 100−200 mg of ZrTe (*MnP*) were loaded into polytetrafluorethylene (KLF) sample holders in an Ar-filled glovebox. Magnetization measurements were carried out between 1.8 and 330 K in fields of 10 and 30 kG. The field dependence of the magnetization was measured at 5 K.

(19) Lide, D. R., Ed. *CRC Handbook of Chemistry and Physics*, 76th ed.; CRC Press: Boca Raton, FL, 1996.

(20) Deslattes, R. D.; Henins, A. *Phys. Rev. Lett.* **1976**, *36*, 898.

(21) Wagner, V.; Degen, T. *DIFFRAKT (V1.0)*, a program for processing X-ray powder data; Universität Bonn, 1995.

(22) STOE & Cie: *X-RED 1.07*, Data reduction for STADI4 and IPDS; *X-SHAPE 1.01*, Crystal optimisation for numerical absorption correction; Darmstadt, 1996.

(23) Sheldrick, G. M. *SHELXL-97*, Program for the refinement of crystal structures; Universität Göttingen, 1997.

(24) Crawford Dunlap, W., Jr. In *Methods of experimental physics*, Vol. 6, Part B: Solid-state physics; Horovitz, K. L., Johnson, V. A., Eds.; Academic Press: New York, 1959; p 33.

(25) Weiss, A.; Witte, H. *Magnetochemie*; VCH: Weinheim, 1973; p 95.

Table 2. Atomic Coordinates and Equivalent (U_{eq}) and Anisotropic Displacement Parameters for ZrTe (*MnP*) (in pm^2)

atom	site	*x*	*y*	*z*	U_{eq}	U_{11}	U_{22}	U_{33}	U_{23}	U_{13}	U_{12}
Te1	4*c*	0.70906(5)	1/4	0.42623(4)	38.7(16)	44(2)	38(2)	34(2)	0	−5.7(10)	0
Zr1	4*c*	0.00829(7)	1/4	0.69123(7)	45.3(17)	43(3)	59(3)	33(3)	0	0.6(15)	0

Table 3. Selected Interatomic Distances (in pm)

Zr1−Te1	1×	287.71(7)	Te1−Zr1	1×	287.71(7)
Zr1−Te1	2×	293.05(6)	Te1−Zr1	2×	293.05(6)
Zr1−Te1	2×	296.66(6)	Te1−Zr1	2×	296.66(6)
Zr1−Te1	1×	304.26(8)	Te1−Zr1	1×	304.26(8)
Zr1−Zr1	2×	325.95(7)	Te1−Te1	2×	376.28(7)
Zr1−Zr1	2×	377.23(8)	Te1−Te1	2×	377.23(8)
Zr1−Zr1	2×	378.5(1)	Te1−Te1	4×	399.71(7)

Table 4. Parameters Used for Extended Hückel Calculations for ZrTe (*MnP*)

orbital		H_{ii} (eV)	ζ_1[a]	c_1[b]	ζ_2[a]	c_2[b]
Zr	5s	−7.942	1.82			
	5p	−4.353	1.78			
	4d	−7.756	3.84	0.6213	1.505	0.5798
Te	5s	−21.20	2.51			
	5p	−12.00	2.16			

[a] Slater-type orbital exponents. [b] Coefficients used in double-ζ expansion.

Electronic Structure Calculations. Band structure calculations on ZrTe (*MnP*) were carried out within the tight-binding approximation, at 96 k points, using the extended Hückel method.[26−28] Valence-state ionization energies (H_{ii}'s) for Zr were obtained from charge-iterative calculations on ZrTe (*MnP*), using fixed valence-state ionization energies for Te. Other parameters were taken from the literature.[29] The parameters are listed in Table 4.

Results and Discussion

Phase Relations, Phase Transition. The lattice parameters determined for ZrTe (*MnP*) prepared and treated with different methods did not point to a homogeneity range. In equiatomic samples prepared in an arc-melting furnace, diffuse reflections of ZrTe (*MnP*) were observed in addition to reflections of Zr_5Te_6[14] and Zr_5Te_4.[17,30] This points to the emergence of ZrTe (*MnP*) during the cooling process. An access of ZrTe (*MnP*) to the melt is considered very unlikely. Differential scanning calorimetry (DSC) experiments in combination with phase analysis with X-ray powder diffraction showed a first-order reconstructive phase transition from ZrTe (*WC*) to ZrTe (*MnP*) at 1438 ± 5 K (1165 °C). The phase transition is reversible, although the reverse reaction is kinetically inhibited. This is shown in Figure 2. ZrTe (*MnP*) is stable up to at least 1770 K. Zr_5Te_4 represents the next metal-rich phase. On the tellurium-rich side Zr_5Te_6 follows ZrTe (*MnP*).

The enthalpy of the phase transition ZrTe (*WC*)−ZrTe (*MnP*) amounts to 8.3 ± 1.0 kJ mol^{-1}. This is somewhat larger than the transition enthalpy of 5.2 ± 0.6 kJ per mol Zr atom, which was determined for a phase transition in Zr_5Te_6 occurring at 1513 ± 5 K.[31] For comparison, the enthalpy of the phase transition α-Zr → β-Zr from hexagonal to body-centered cubic at 1139 K amounts to 4.1 kJ mol^{-1}.[32]

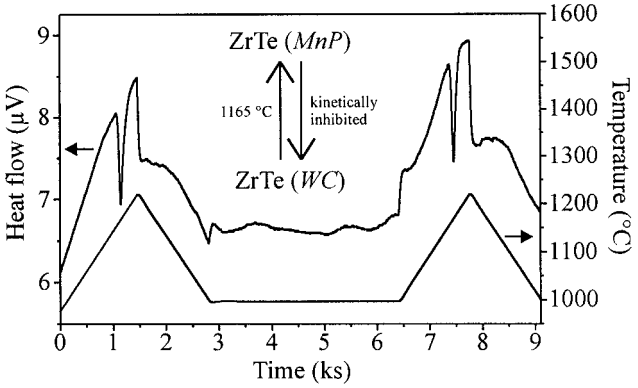

Figure 2. DSC recording of the phase transition ZrTe (*WC*)-ZrTe (*MnP*) at 1165 °C. Two heating cycles up to 1225 °C are shown. The endothermic enthalpy effect of the transition is clearly visible in the heating segments. During cooling, an exothermic effect of a reverse transition is not observed. Holding the temperature at 1000 °C for 1 h affords a complete reverse transition; both peaks are of equivalent area. The phase transition can be performed repeatedly on the same sample. Note that the heat flow changes abruptly upon changes in heating rate (switching effect). Heating and cooling rates were 10 °C min^{-1}.

As an examination of the interatomic distances as well as a bonding analysis show (see below), formally one out of three Zr−Zr bonds in the hexagonal plane of ZrTe (*WC*) has to be broken in the course of the phase transition ZrTe (*WC*)−ZrTe (*MnP*). One further Zr−Zr bond, as well as the total Zr−Te interactions must be weakened. On the opposite side, due to the zigzag chain formation, the third Zr−Zr bond gains considerably in strength. Thus, in the first approximation, the measured endothermic enthalpy effect could be understood as the difference between the mentioned loss and gain terms. This is maintained without the intention of explaining or elucidating the transition mechanism in any way.

During our investigations, we have not been able to confirm reports on NiAs−WC type dimorphism in ZrTe,[16,33] neither have we been able to verify the existence of a NiAs type phase in the Zr−Te system. Apart from ZrTe, a NiAs−WC type dimorphism has been reported in NbS, NbN, and TiS.[34] Those reports, however, have not been confirmed. NbS was described in the Introduction.[10] NbN transfers at high temperatures from a tetragonal to a cubic, NaCl type phase.[35] TiS probably exclusively crystallizes in the NiAs type.[36,37]

Structure maps provide an empirical basis for predicting the structure types adopted by various compounds.[38−40] For example, Villars has constructed a three-dimensional structural stability diagram for AB compounds,[39] plotting the difference of Zunger's pseudopotential radii sums, the Martynov−Batsanov

(26) Hoffmann, R. *J. Chem. Phys.* **1963**, *39*, 1397.
(27) Whangbo, M.-H.; Hoffmann, R. *J. Am. Chem. Soc.* **1978**, *100*, 6093.
(28) Köckerling, M. *Program EHMACC*, adapted for use on PC by M. Köckerling, Gesamthochschule Duisburg, 1997.
(29) Clementi, E.; Roetti, C. *At. Data Nucl. Data Tables* **1974**, *14*, 177.
(30) Örlygsson, G.; Harbrecht, B. *Z. Kristallogr.−NCS* **1999**, *214*, 5.
(31) Örlygsson, G. Low-valent zirconium tellurides, Ph.D. Dissertation Thesis, Philipps-Universität Marburg, 2000.
(32) Guillermet, A. F. *High Temp.−High Press.* **1987**, *19*, 119.
(33) Sodeck, H.; Mikler, H.; Komarek, K. L. *Monatsh. Chem.* **1979**, *110*, 1.
(34) (a) Villars, P. *Pearson's Handbook*, desk ed.; American Society for Metals: Materials Park, OH, 1997. (b) Villars, P.; Calvert, L. D. *Pearson's Handbook of Crystallographic Data for Intermetallic Phases*, 2nd ed.; American Society for Metals: Materials Park, OH, 1991.
(35) Kim, S.-J.; Franzen, H. F. *J. Less-Common Metals* **1988**, *143*, 339.
(36) Wiegers, G. A.; Jellinek, F. *J. Solid State Chem.* **1970**, *1*, 519.
(37) Onoda, M.; Wada, H. *J. Less-Common Metals* **1987**, *132*, 195.
(38) Mooser, E.; Pearson, W. B. *Acta Crystallogr.* **1959**, *12*, 1015.
(39) Villars, P. *J. Less-Common Metals* **1983**, *92*, 215.
(40) Zunger, A. *Phys. Rev.* **1980**, *B12*, 5839.

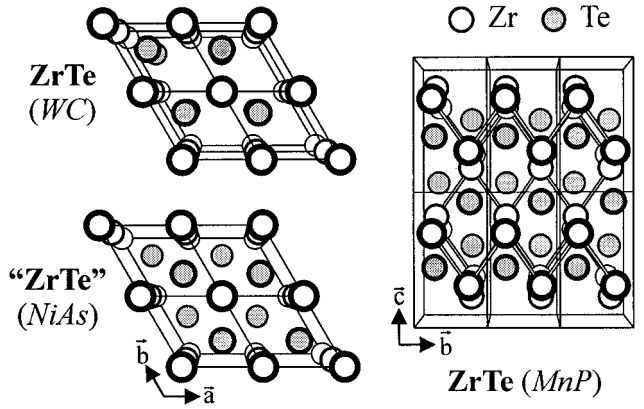

Figure 3. Central projection of the ZrTe (*MnP*) structure parallel to the crystallographic *a*-axis. The short Zr−Zr contacts in the zigzag chains are emphasized. For comparison, the structures of ZrTe (*WC*) and hypothetical ZrTe (*NiAs*) are shown. The line thickness of the atoms represents their position (height) above the plane. Unit cells are indicated with lines.

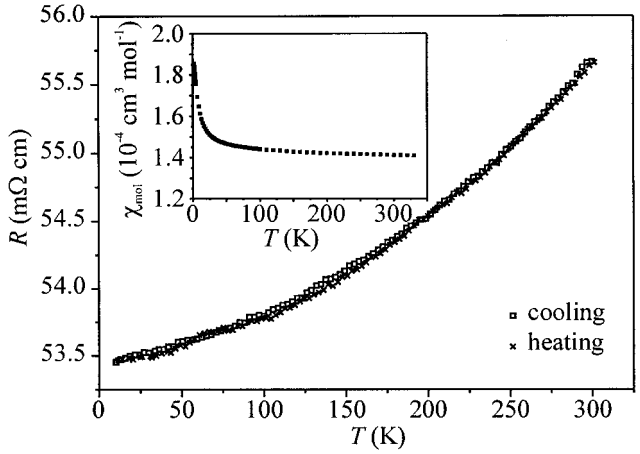

Figure 4. Temperature dependence of the electrical resistivity of ZrTe (*MnP*). $I = 8$ mA. Inset: Temperature dependence of the molar magnetic susceptibility of a powder sample of ZrTe (*MnP*) measured at a field of 30 kG.

electronegativity difference, and the sum of the number of valence electrons. In this diagram, polymorphous compounds are expressed through an overlap of the volumes of two or three structure types. Interestingly, the WC and MnP structure types lie side by side, allowing for the possibility of a phase transition. ZrTe lies near the suggested boundary surface between both structure types. Considering the present results for the structures adopted by ZrTe, a partial overlap of both volumes has to be assumed. As mentioned earlier, a WC−MnP type dimorphism is reported here for the first time.

Structural Features. ZrTe (*MnP*) crystallizes in the MnP type structure[5] (Figure 3). In the zigzag chains, which extend parallel to [010], the shortest Zr−Zr distances in the structure are found, 326.0 pm. This distance is comparable to the shortest Zr−Zr distance in Zr_5Te_6 (326.4 pm).[14] The second Zr−Zr contact inside the chains amounts to 377.2 pm, almost identical to the Zr−Zr distance in the hexagonal planes in ZrTe (*WC*). The Zr−Zr distance between the zigzag chains is 468.6 pm and corresponds approximately to the distance between the Zr_7 clusters in Zr_5Te_6, 470.5 pm. The Zr−Zr distance "parallel" to [100] amounts to 378.5 pm. The coordination sphere of the Zr atoms can be seen as a distorted octahedral one, with $d_{Zr-Te} =$ 287.7−304.3 pm, whereas the Te atoms are distorted trigonal prismatically surrounded with Zr atoms. The Te−Te contacts are ≥376.3 pm, pointing to van der Waals interactions.

A comparison of the lattice parameters of ZrTe (*MnP*) and ZrTe (*WC*) elucidates the geometrical relations between both structures. The *a*-lattice parameter corresponds to the doubled *c*-lattice parameter of ZrTe (*WC*) ($2 \times c_{WC} = 772.1$ pm). The *b*-lattice parameter is directly comparable to the *a*-parameter of ZrTe (*WC*) ($a_{WC} = 377.1$ pm). The *c*-parameter stands in a $3^{1/2}$-relation to the *a*-parameter of ZrTe (*WC*) ($3^{1/2} \times a_{WC} =$ 653.1 pm). One recognizes that the crystallographic *a*-axis is shortened (4.3%), the *b*-axis stays unchanged, and the *c*-axis is elongated (6.3%), as compared to the transformed lattice dimensions of ZrTe (*WC*). The cell volume per formula unit (ZrTe) increases slightly from ZrTe (*WC*) (47.5×10^6 pm^3) to ZrTe (*MnP*) (48.4×10^6 pm^3). The shortening of the crystallographic *a*-axis can be related to the shifting of the atoms away from the rigid, trigonal prismatic AbAb-arrangement of the WC type structure. The relaxation to the MnP type structure, which is derived from the hexagonal close-packed arrangement of the nonmetal atoms (A, B) in the NiAs type, AcBcAc, allows this change to take place. Compared to ZrTe (*WC*) half of the Zr−Zr bonds perpendicular to the zigzag chains (parallel to [001]) are broken. This is expressed in an elongation of the structure in the [001] direction.

A further result of the relaxation of the ZrTe (*WC*) structure to the ZrTe (*MnP*) structure is a corrugation of the Te atom layers, with an amplitude of approximately 60 pm in the [100] direction. This is connected to the "cleft" between the Zr atom zigzag chains; the Te atoms shift toward and into those "clefts".

Up to now, only one telluride crystallizing in the MnP type has been reported. MnTe crystallizes under normal conditions in the NiAs type. According to high-pressure X-ray powder diffraction experiments, the MnP type structure occurs reversibly above 24 GPa, after the appearance of an intermediate phase.[41] The structure of MnTe (*MnP*) contains strikingly short Te−Te distances of 316.2 pm, intermediate between the two shortest distances in elemental Te, 283.5 and 349.5 pm.[42] This could be attributed to the formation of Te−Te bonding interactions under pressure. Similar Te−Te distances are found for example in $ZrTe_3$, where bonding Te−Te interactions are observed.[43,44] According to that, the high-pressure modification of MnTe differs fundamentally from ZrTe (*MnP*) with regard to the crystallographic as well as the electronic structure.

Physical Properties. As can be seen in Figure 4, the resistivity rises with temperature, pointing to a metallic behavior of ZrTe (*MnP*). For a metallic compound, however, the resistivity is unusually high, $\rho_{10K} = 53.5$ mΩ cm and $\rho_{300K} =$ 55.7 mΩ cm, compared to, e.g., the same data for Zr ($\rho_{10K} =$ 0.253×10^{-3} mΩ cm; $\rho_{300K} = 43.3 \times 10^{-3}$ mΩ cm).[19] The resistivity of a $ZrTe_2$ single crystal at 300 K was reported as 0.5 mΩ cm.[45] In addition, the residual resistance ratio of this metallic conducting compound is much higher than that for ZrTe (*MnP*), $\rho_{300K}/\rho_{4K} = 7-15$ ($ZrTe_2$), compared to $\rho_{300K}/\rho_{10K} =$ 1.04 (ZrTe (*MnP*)). Apart from real specific features regarding the transport properties, grain boundary effects in the powder samples could, among others, be made responsible for the high measured resistances.

The inset in Figure 4 shows the temperature dependence of the magnetic susceptibility of ZrTe (*MnP*) at 30 kG. The

(41) Mimasaka, M.; Sakamoto, I.; Murata, K.; Fujii, Y.; Onodera, A. *J. Phys. C: Solid State Phys.* **1987**, *20*, 4689.
(42) Cherin, P.; Unger, P. *Acta Crystallogr.* **1967**, *23*, 670.
(43) Felser, C.; Finckh, E. W.; Kleinke, H.; Rocker, F.; Tremel, W. *J. Mater. Chem.* **1998**, *8*, 1787.
(44) Stöwe, K.; Wagner, F. R. *J. Solid State Chem.* **1998**, *138*, 160.
(45) Aoki, Y.; Sambongi, T.; Levy, F.; Berger, H. *J. Phys. Soc. Jpn.* **1996**, *65*, 2590.

observed, essentially temperature independent paramagnetic susceptibility ($\chi_{mol} = 0.14 \times 10^{-3}$ cm^3 mol^{-1}) is typical for materials with metallic transport properties resulting from unpaired conduction electrons. A field-independent susceptibility was obtained at 5 K.

Chemical Bonding in MnP, NiAs, and WC Type ZrTe: A Comparison. In AB carbides and nitrides of the transition metals, the WC type structure is adopted for valence-electron counts of 10 per formula unit.[1] Examples are WC and TaN (W and Ta d^2). In AB phosphides the NiAs type structure is dominant for 9 and 10 valence electrons per formula unit, whereas for 11−14 valence electrons the MnP type structure is observed.[2] An example is MoP (11 valence electrons, d^3). ZrTe contains 10 valence electrons per formula unit and can, accordingly, be expected to adopt the WC type structure. Bearing in mind the structures adopted by the phosphides, one could have expected a transition to a NiAs type phase at higher temperatures. Apparently, with the possibility of stabilization through the formation of metal atom zigzag chains, this alternative becomes superfluous. The gain in bonding energy upon the emergence of the zigzag chains is seemingly preferred to the intuitively expected increase (at least retention) of symmetry on moving from the low- to high-temperature phase, which would have been achieved with the formation of ZrTe (*NiAs*).

The influence of the d-electron count on clustering in chalcogenides of the valence electron poor transition metals,[46] including some zirconium tellurides, has been discussed elsewhere.[14] The arrangement of the metal atoms to zigzag chains is typical for phases with a d^2 metal atom electron configuration. ZrTe counts to those phases. Other representatives are for example α- and β-ZrI_2,[47,48] and β-$MoTe_2$.[49] To learn more about the factors influencing the adopted structure type, in the following, the results of extended Hückel calculations on MnP, NiAs, and WC type ZrTe are compared.

According to the total density of states (DOS) for ZrTe (*MnP*) shown in Figure 5a, the Fermi level (ϵ_F) lies in a region that is governed by Zr d-orbital contributions. This is in accordance with the observed metallic behavior. The Te p-orbital contributions extend downward from about 2.5 eV below ϵ_F. Comparing the DOS for ZrTe (*MnP*) and the undistorted, hypothetical ZrTe (*NiAs*) (Figure 5b)[18] clearly shows the advantages of the MnP type structure. Zr d-electron density is shifted to lower energies, the ϵ_F lying close to a local DOS minimum. As compared to the DOS for the low-temperature hexagonal form, ZrTe (*WC*) (Figure 5c),[18] the d-block of ZrTe (*MnP*) also is shifted slightly to lower energies. Thus, in the high-temperature orthorhombic form, ZrTe (*MnP*), there are significantly more Zr d-states available for homonuclear bonding interactions than in both ZrTe (*WC*) and ZrTe (*NiAs*).

Figure 5d shows the COOP diagrams for homonuclear Zr−Zr interactions as well as heteronuclear Zr−Te interactions in ZrTe (*MnP*). On the basis of the COOP diagrams it can be seen that the heteronuclear interactions make up the main component of the bonding interactions. In Figure 5e, a projection of the COOP curve for the short distance in the zigzag Zr atom chain is shown. It becomes apparent that here the main part of the bonding Zr−Zr interactions is to be found. An analysis of the Mulliken overlap populations (MOP) in a structure allows a relative quantification of the bonding interactions. Table 5 shows the MOP values for ZrTe (*MnP*). Corresponding values for ZrTe (*NiAs*) and ZrTe (*WC*) have been reported.[18] Here the importance of the bonds in the zigzag chain as compared to other Zr−Zr interactions again becomes clear. The MOP value of the short contacts in the zigzag chain amounts to 0.273 as opposed to 0.071 and 0.054 for the other two bonding interactions. An examination of the MOP value for the second contact inside the zigzag chain (0.071; 377.2 pm) is interesting. Retaining the

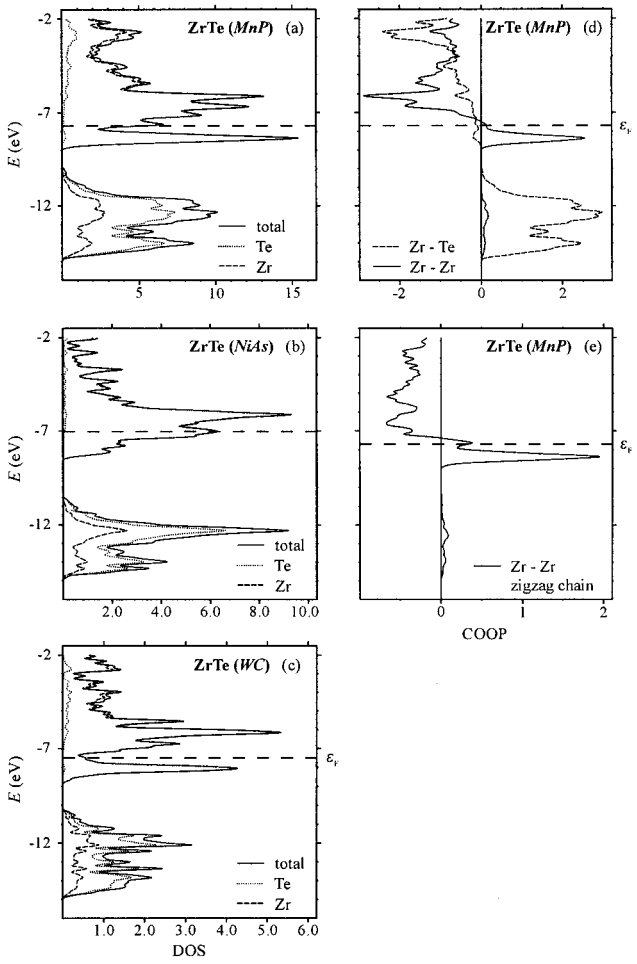

Figure 5. Densities of states (DOS) (a−c) and crystal orbital overlap population (COOP) curves (d−e). Levels up to the Fermi level (ϵ_F, broken, horizontal line) are filled; levels to the right of the vertical line in the COOP curves are bonding, those to the left are antibonding. (a) DOS for ZrTe (*MnP*), $\epsilon_F = -7.7$ eV. (b) DOS for ZrTe (*NiAs*), $\epsilon_F = -7.0$ eV. (c) DOS for ZrTe (*WC*), $\epsilon_F = -7.5$ eV. (d) COOP curves for ZrTe (*MnP*). COOP curves for Zr−Te and Zr−Zr contacts up to 305 and 379 pm, respectively, are shown. (e) The projected COOP curve for the short contact (325.95 pm) in the Zr atom zigzag chain of ZrTe (*MnP*).

Table 5. Interatomic Distances and Mulliken Overlap Populations (MOP) for ZrTe (*MnP*)

ZrTe (*MnP*)		*d* (pm)	MOP	MOP per "bond"
Zr−Te	4×	287.71	1.444	0.361
Zr−Te	8×	293.05	2.843	0.355
Zr−Te	8×	296.66	2.769	0.346
Zr−Te	4×	304.26	1.333	0.333
Zr−Zr zigzag	4×	325.95	1.092	0.273
Zr−Zr parallel *b*	4×	377.23	0.282	0.071
Zr−Zr parallel *a*	4×	378.5	0.215	0.054
		Zr−Te total/4 = 2.097[a]		
		Zr−Zr total/4 = 0.397[b]		

[a] For ZrTe (*WC*): 2.152. For ZrTe (*NiAs*): 2.280.[18] [b] For ZrTe (*WC*): 0.355. For ZrTe (*NiAs*): 0.233.[18]

(46) Rouxel, J. *Chem. Eur. J.* **1996**, *2*, 1053.
(47) Guthrie, D. H.; Corbett, J. D. *J. Solid State Chem.* **1981**, *37*, 256.
(48) Corbett, J. D.; Guthrie, D. H. *Inorg. Chem.* **1982**, *21*, 1747.
(49) Brown, B. E. *Acta Crystallogr.* **1966**, *20*, 268.

same distance, this interaction turns out to be noticeably weaker than the one in ZrTe (*WC*) (0.103; 377.1 pm).[18] A comparison of the integral MOP values for ZrTe (*WC*) and ZrTe (*MnP*) shows a distinct strengthening of the homonuclear Zr−Zr bonds in ZrTe (*MnP*) as opposed to ZrTe (*WC*) (0.355 vs 0.397). The heteronuclear bonds become somewhat weaker (2.152 vs 2.097).

No covalent bonding nonmetal−nonmetal interactions could be established for ZrTe (*MnP*) ($-0.02 \leq$ MOP/atom pair ≤ 0). In this respect ZrTe (*MnP*) differs from phosphides and arsenides exhibiting this structure type.[2]

An examination of the MOP values, in context with the DOS diagrams in Figure 5, for hypothetical ZrTe (*NiAs*) as compared to ZrTe (*WC*) and ZrTe (*MnP*) underlines the importance of the bonding interactions occurring in the vicinity of the Fermi level: Despite the dominance of heteronuclear interactions in the total bonding interactions in all three phases, the small variations in homonuclear interactions just below the Fermi level are decisive as to which structure is formed. As mentioned, we have not been able to verify the existence of a NiAs type ZrTe.[16,33]

Conclusions

At equiatomic composition in the system Zr−Te a new high-temperature phase was uncovered. ZrTe crystallizes in a distorted NiAs type structure of the MnP type, in which the Zr atoms are arranged to zigzag chains. The low-temperature phase crystallizes in the WC type. The reconstructive phase transition from ZrTe (*WC*) to ZrTe (*MnP*) occurs at 1438 K and is of first order. The transition proceeds reversibly, but is kinetically inhibited. A WC−MnP type phase transition has not been reported before. ZrTe (*MnP*) shows the properties of a poor metallic conductor with an almost temperature independent paramagnetic susceptibility. As compared to ZrTe (*WC*), extended Hückel calculations reveal a distinct increase in bonding Zr−Zr interactions. This is attributed to the strong contacts in the Zr atom zigzag chains and is understood as the driving force of the transition. Metal atom zigzag chains are observed in pnictides, chalcogenides, and halides of valence electron poor transition metals in which a d^2 electron configuration is realized. This is also the case in ZrTe.

Acknowledgment. Financial support by the Deutsche Forschungsgemeinschaft and the Fonds der Chemischen Industrie is gratefully acknowledged. We would like to thank Mr. Rüdiger Penzel for assistance with the DSC measurements.

Supporting Information Available: A table of additional crystallographic and refinement data and tables of relevant parameters of the Rietveld analysis with a listing of 2θ values, indexation, and calculated and observed relative X-ray diffraction intensities (PDF) and an X-ray crystallographic file (CIF). This material is available free of charge via the Internet at http://pubs.acs.org.

JA004164R